Acceleration of raindrop formation due to the tangling-clustering instability in a turbulent stratified atmosphere

T. Elperin,[1,*] N. Kleeorin,[1,†] B. Krasovitov,[1,‡] M. Kulmala,[2,§] M. Liberman,[3,4,∥] I. Rogachevskii,[1,¶] and S. Zilitinkevich[2,5,6,7,**]

[1]*The Pearlstone Center for Aeronautical Engineering Studies, Department of Mechanical Engineering, Ben-Gurion University of the Negev, P. O. Box 653, Beer-Sheva 84105, Israel*

[2]*Division of Atmospheric Sciences, Department of Physics, P. O. Box 64, 00014 University of Helsinki, Finland*

[3]*Nordita, KTH Royal Institute of Technology and Stockholm University, Roslagstullsbacken 23, 10691 Stockholm, Sweden*

[4]*Moscow Institute of Physics and Technology, Dolgoprudnyi, 141700, Russia*

[5]*Finnish Meteorological Institute (FMI) P. O. Box 503, 00101 Helsinki, Finland*

[6]*Department of Radio Physics, N. I. Lobachevsky State University of Nizhny Novgorod, Russia*

[7]*Moscow State University; Institute of Geography of Russian Academy of Sciences, Moscow, Russia*

(Received 26 January 2015; revised manuscript received 21 April 2015; published 13 July 2015)

Condensation of water vapor on active cloud condensation nuclei produces micron-size water droplets. To form rain, they must grow rapidly into at least 50- to 100-μm droplets. Observations show that this process takes only 15–20 min. The unexplained physical mechanism of such fast growth is crucial for understanding and modeling of rain and known as "condensation-coalescence bottleneck in rain formation." We show that the recently discovered phenomenon of the tangling clustering instability of small droplets in temperature-stratified turbulence [Phys. Fluids **25**, 085104 (2013)] results in the formation of droplet clusters with drastically increased droplet number densities. The mechanism of the tangling clustering instability is much more effective than the previously considered by us the inertial clustering instability caused by the centrifugal effect of turbulent vortices. This is the reason of strong enhancement of the collision-coalescence rate inside the clusters. The mean-field theory of the droplet growth developed in this study can be useful for explanation of the observed fast growth of cloud droplets in warm clouds from the initial 1-μm-size droplets to 40- to 50-μm-size droplets within 15–20 min.

DOI: 10.1103/PhysRevE.92.013012 PACS number(s): 47.27.tb, 47.55.Hd

I. INTRODUCTION

When an ascending parcel of moist air reaches the condensation level, an initial mist of small, micron-size water droplets is formed, which are suspended in the air. In the supersaturated environment water droplets grow due to condensation of water vapor from the surrounding atmosphere. However, to form the raindrops, which can fall down, triggering rain, they must grow to about 50-μm-size droplets, which would take a very long time. Observations indicate that the average time for rainfall initiation is approximately 15–20 min, while existing theories predict that the duration of a time interval required for droplets to grow up to 50 μm in radius is of the order of hours (see, e.g., reviews in Refs. [1–3] and references therein). Indeed, although the actual time to form large droplets depends on the initial droplet size spectrum and cloud water content (see, e.g., [4]), the predicted growth time differs considerably from the observations.

Initiation of rain in turbulent clouds comprises three stages. The first stage involves condensation of water vapor on cloud condensation nuclei (CCN; typically having a size of the order of 0.05 μm) and formation of small micron-size droplets. At the next stage, droplets grow efficiently through condensation and diffusion of water vapor and may attain radii of about 10 μm. It is generally believed that droplets having radii larger than 50 μm fall out of the cloud due to gravitational sedimentation and continue to grow in size mainly through gravitational collisions into rain droplets with the size of the order of 80–100 μm. Understanding a mechanism of rapid growth of initially small droplets to the size of the order of 50 μm when gravitational collision-coalescence becomes effective is still poorly understood and remains a subject of active research (see, e.g., Refs. [1–3]). Identifying mechanisms of rapid growth of cloud droplets and determining the growth rate, i.e., theoretical explanation of the "*size gap or the condensation-coalescence bottleneck in warm rain formation*" [3] is one of the major challenges in cloud physics.

Observations show the existence of strong turbulence in clouds. Different mechanisms have been suggested and different aspects of turbulence effects on the growth of cloud droplets have been considered to explain the rapid formation of rain droplets in clouds [3]. These mechanisms involve, e.g., effects of giant aerosol particles for faster formation of large cloud droplets, thereby initiating coalescence sooner [5], and droplet spectra broadening under conditions of water vapor supersaturation [6–8]. Numerous theoretical, numerical, and experimental studies have used different approaches and models to investigate the effects of atmospheric turbulence on growth of cloud droplets by collision-coalescence and formation of rain droplets (see Refs. [1–3], and references therein).

Most of the studies have focused on amplification of the fall velocity of cloud droplets in turbulent atmosphere and turbulence induced increase of the droplet collision kernel. Air turbulence can enhance droplet coalescence rate by increasing the relative velocity of droplets due to differential acceleration

*elperin@bgu.ac.il; http://www.bgu.ac.il/me/staff/tov

†nat@bgu.ac.il

‡borisk@bgu.ac.il

§markku.kulmala@helsinki.fi

∥misha.liberman@gmail.com; http://michael-liberman.com/

¶gary@bgu.ac.il; http://www.bgu.ac.il/~gary

**sergej.zilitinkevich@fmi.fi

and enhance collision kernel of cloud droplets. For example, when the dissipation rate of turbulence is increased from 100 to 400 $\text{cm}^2\ \text{s}^{-3}$, the droplet coalescence rate (between droplets with the sizes 18 and 20 μm) increases by a factor of 3.5 [9]. The increase of droplet relative velocity and local accumulation of inertial droplets near the periphery of turbulent eddies due to centrifugal effect can increase the droplet collision rate (see, e.g., Refs. [1,9–25]). Numerical simulations showed that due to the effect of preferential concentration of inertial particles in turbulent flows their settling rate is about 20% larger than the terminal fall velocity in the quiescent atmosphere (see, e.g., Refs. [1,10,14,15,18,20,21,26]). This list of references is obviously not complete because the topic is a subject of intense ongoing research and has attracted the attention of numerous researchers (see, e.g., Refs. [2,3]).

Accurate modeling of droplet collision-coalescence is important because collisions strongly affect droplet size, velocity distributions, and dispersion of droplets [27]. Droplet collisions may have numerous outcomes—the droplets might smoothly merge with little deformation, bounce off each other, coalesce following large deformation, or separate after temporarily coalescing. Many of the used droplet interaction models assume that droplet velocities before collisions are not correlated. However, this assumption is violated in turbulent flows. Indeed, small droplets have low inertia and follow almost the same trajectories as fluid particles and, therefore, their precollision velocities are strongly correlated with the velocity of a carrying fluid [28]. Many of the studies focused on collisions between identical droplets whereby the collision outcome depends on the impact parameter and the ratio of kinetic energy to surface tension. It was demonstrated that size disparity can significantly increase the parameter range over which droplets permanently coalesce [29].

Dynamics and interactions of liquid droplets, and their collisions, coalescence, and bouncing, become more significant with an increase of their size and are encountered in many naturally occurring phenomena and industrial applications, including rain initiation and combustion. Nevertheless, the collision rate for typical droplet number densities in clouds is too far from being sufficient for their efficient coalescence. The general opinion is that turbulence somehow enhances droplet collision rate and droplet coalescence. However, it still remains unclear and not completely established yet to what extent and how turbulence can affect and control droplet coalescence and rain initiation (see, e.g., Refs. [2,3]).

In this paper we explain the fast growth of cloud droplets by collision-coalescence, taking into account the recently discovered phenomenon of the tangling clustering instability of small water droplets in turbulent temperature-stratified atmosphere [30]. We assume that water droplets coalesce after collisions. However, the ambient mean number density of the droplets is too low, so their collision-coalescence time is very large. The situation dramatically changes in the presence of tangling clustering instability, which results in the formation of clusters with the mean number density of the droplets inside the clusters that by several orders of magnitude exceeds the ambient mean number density of the droplets.

The mechanism of droplet clustering in turbulence is as follows. Due to inertia effects droplets inside turbulent eddies are carried out to the boundary between the eddies by inertial forces. Therefore, water droplets are locally accumulated in the regions with low vorticity and maximum pressure fluctuations [31]. Contrary to the inertia induced preferential concentration, the pressure fluctuations in stratified turbulence with a nonzero mean temperature gradient are increased due to additional temperature fluctuations generated by tangling of the mean temperature gradient by velocity fluctuations. This is a reason why clustering of water droplets is much more effective in stratified turbulence [30,32] in comparison with a nonstratified turbulence [12].

The tangling clustering instability leads to the formation of clusters, which accumulate surrounding droplets. Since the number density and, correspondingly, the collision-coalescence rate of small droplets inside the clusters drastically increase, the characteristic time of droplet coalescence sharply decreases. The effect of the tangling clustering instability [30] is much stronger than that of the inertial clustering instability [12] in nonstratified isotropic and homogeneous turbulence. The strong enhancement of the droplet collision-coalescence rate caused by the effect of the tangling clustering instability of small droplets can explain the observed fast growth of cloud droplets from the initial 1-μm-size droplets to 40- to 50-μm size droplets within 15–20 min.

II. TANGLING CLUSTERING INSTABILITY

Small cloud droplets with a size of the order of 1 μm have to grow in diameter by a factor 50–100 in order to fall out of the cloud as rain droplets. Initial formation of cloud droplets is associated with an intricate process that allows conversion of water vapor into small liquid water droplets. Droplet formation always requires the presence of aerosols and their activation to cloud droplets and further growth of droplets via condensation-coalescence. Clearly, the growth of cloud droplets is constrained by their vaporization, and droplet collisions and coalescence may modify the droplet size distribution (see, e.g., Refs. [33–35]).

In the present study we invoke the recently discovered phenomenon of tangling clustering instability of droplets in temperature-stratified turbulence which causes formation of clusters with the droplet number density inside the clusters by several orders of magnitude larger than the ambient droplet number density [30]. The size of the formed clusters is of the order of the Kolmogorov microscale length. For the sake of simplicity in this section we assume that vapor condensation produces small droplets of the same size, which then grow due to the collision-induced coalescence. The droplet size distribution is taken into account in the next section.

A. Governing equations

The theory of the tangling clustering instability in the temperature-stratified turbulence has been developed in Ref. [30]. In this section we summarize these theoretical results and explain why the clustering instability is essentially enhanced in turbulence with a large-scale temperature gradient. Equation for the instantaneous number density $n(t,\boldsymbol{r})$ of small spherical droplets in a turbulent flow reads:

$$\frac{\partial n}{\partial t} + \nabla\cdot(n\,\boldsymbol{v}) = D_m\,\Delta n - \frac{n}{\tau_{\rm ev}} + I_0, \qquad (1)$$

where $D_m = k_B\,T/(3\pi\rho\,\nu\,d)$ is the coefficient of molecular (Brownian) diffusion of droplets having diameter d and the instantaneous velocity $\boldsymbol{v}(t,\boldsymbol{r})$, ν is the kinematic viscosity, T and ρ are the mean air temperature and density, k_B is the Boltzman constant, and I_0 is the rate of production of the droplets number density caused by an external source of droplets, e.g., through activation. The term $-n/\tau_{\rm ev}$ in the right-hand side of Eq. (1) describes the decrease of the droplet number density due to the evaporation, where $\tau_{\rm ev}$ is the characteristic evaporation time determined by Eq. (26) in Sec. III B, see, e.g., Ref. [36].

The droplet velocity $\boldsymbol{v}$ is determined by the equation of motion:

$$\frac{d\boldsymbol{v}}{dt} = \frac{\boldsymbol{u}-\boldsymbol{v}}{\tau_{\rm st}} + \boldsymbol{g}. \qquad (2)$$

Here $\boldsymbol{u}(t,\boldsymbol{x})$ is the fluid velocity and $\boldsymbol{g}$ is the gravity acceleration, $\tau_{\rm st} = m_{\rm dr}/3\pi\rho\,\nu\,d$ is the Stokes time, $m_{\rm dr} = (\pi/6)\,\rho_m\,d^3$ is the droplet mass, and $\rho_m \gg \rho$ is the droplet mass density. The ratio ${\rm St} = \tau_{\rm st}/\tau_\eta = \rho_m\,d^2/18\rho\,\ell_\eta^2$, of the Stokes time and the Kolmogorov turbulent turnover time, τ_η, is the Stokes number, where $\tau_\eta = \ell_\eta/u_\eta = \tau_0/{\rm Re}^{1/2}$, $u_\eta = u_0/{\rm Re}^{1/4}$ is the characteristic velocity of eddies in the Kolmogorov microscale, $\ell_\eta = \ell_0/{\rm Re}^{3/4}$, ${\rm Re} = u_0\ell_0/\nu$ is the Reynolds number, u_0 is the characteristic turbulent velocity in the integral turbulent scale ℓ_0, and $\tau_0 = \ell_0/u_0$ is the turbulent time in the integral turbulent scale.

The solution of Eq. (2) for ${\rm St} \ll 1$ reads (see, e.g., Ref. [31]):

$$\boldsymbol{v} = \boldsymbol{u} - \tau_{\rm st}\left[\frac{\partial \boldsymbol{u}}{\partial t} + (\boldsymbol{u}\cdot\nabla)\boldsymbol{u} - \boldsymbol{g}\right] + {\rm O}\big(\tau_{\rm st}^2\big). \qquad (3)$$

This equation implies that $\nabla\cdot\boldsymbol{v} \neq 0$, i.e., the droplet velocity field is compressible,

$$\nabla\cdot\boldsymbol{v} = \nabla\cdot\boldsymbol{u} - \tau_{\rm st}\,\nabla\cdot\left(\frac{d\boldsymbol{u}}{dt}\right) + {\rm O}\big(\tau_{\rm st}^2\big)$$
$$= -\frac{1}{\rho}\,(\boldsymbol{u}\cdot\nabla)\rho + \frac{\tau_{\rm st}}{\rho}\,\nabla^2 p + {\rm O}\big(\tau_{\rm st}^2\big). \qquad (4)$$

In the derivation of Eq. (4) we used the Navier-Stokes equation for the fluid. The mechanism of the clustering instability is associated with the droplet inertia. The centrifugal forces cause the droplets inside the turbulent eddies to drift out to the boundary between the eddies, i.e., to the regions with the maximum fluid pressure fluctuations. Indeed, for a large Peclet number, when the molecular diffusion of droplets in Eq. (1) can be neglected, we can estimate $dn/dt \propto -\nabla\cdot\boldsymbol{v}$. Here we neglected evaporation and consider the case $I_0 = 0$. Since $\nabla\cdot\boldsymbol{v} \propto (\tau_{\rm st}/\rho)\,\nabla^2 p \neq 0$ even for incompressible fluid, this implies that $dn/dt \propto -(\tau_{\rm st}/\rho)\,\nabla^2 p > 0$ in the regions where $\nabla^2 p < 0$. Therefore, the droplets are accumulated in regions with maximum pressure fluctuations.

Averaging Eq. (1) over an ensemble of turbulent velocity field, we obtain the following equation for the mean number density of droplets $N = \langle n\rangle$:

$$\frac{\partial N}{\partial t} + \nabla\cdot(N\,\boldsymbol{V}_p + \langle n'\,\boldsymbol{v}'\rangle) = D_m\,\Delta N - \frac{N}{\tau_{\rm ev}} + I_0, \qquad (5)$$

where $\boldsymbol{v}'$ and n' are the fluctuations of the droplet velocity and number density, respectively, and $\boldsymbol{V}_p$ is the mean droplet velocity that is the sum of the mean fluid velocity, $\boldsymbol{U}$, and the terminal fall velocity of droplets, $\boldsymbol{V}_g = \boldsymbol{g}\tau_{\rm st}$ [see Eq. (3)].

The clustering instability of droplets in turbulent flow is determined by fluctuations of the droplet number density, $n'(t,\boldsymbol{r}) = n(t,\boldsymbol{r}) - N(t,\boldsymbol{r})$. Equation for the fluctuations n' is obtained by subtracting Eq. (5) from Eq. (1) [30]:

$$\frac{\partial n'}{\partial t} + \nabla\cdot[n'\,(\boldsymbol{v}' + \boldsymbol{V}_p) - \langle n'\,\boldsymbol{v}'\rangle] - D_m\,\Delta n'$$
$$= -(\boldsymbol{v}'\cdot\nabla)N - N\,\nabla\cdot\boldsymbol{v}' - \frac{n'}{\tau_{\rm ev}}. \qquad (6)$$

B. Mechanism of tangling clustering instability

In a case of temperature-stratified turbulence with a nonzero large-scale temperature gradient, the turbulent heat flux $\langle \boldsymbol{u}'\,\theta\rangle$ is not zero, where $\boldsymbol{u}'$ are the fluctuations of the fluid velocity. This implies correlation between fluctuations of fluid temperature, θ, and velocity, and, therefore, the correlation between fluctuations of pressure and fluid velocity. In temperature-stratified turbulence there are additional pressure fluctuations caused by the tangling of the mean temperature gradient by the velocity fluctuations. This causes the increase of pressure fluctuations and, correspondingly, enhances the droplet clustering. The tangling clustering mechanism is dynamically similar to the inertial clustering mechanism. In particular, the inertial particles drift out to the regions with higher pressure fluctuations, i.e., the regions with lower vorticity and higher strain rate. However, in the temperature-stratified turbulence the pressure fluctuations are stronger than in nonstratified turbulence. Since the clustering is related to the Laplacian of the pressure [see Eq. (12) below] this is the reason for the enhanced tangling clustering.

Fluctuations of the droplet number density are described by the two-point second-order correlation function, $\Phi(t,\boldsymbol{R}) = \langle n'(t,\boldsymbol{x})n'(t,\boldsymbol{x}+\boldsymbol{R})\rangle$. The analysis of the tangling clustering instability employs the equation for the correlation function $\Phi(t,\boldsymbol{R})$ that has been derived using the path-integral approach for random compressible flow with a finite correlation time [12]:

$$\frac{\partial \Phi}{\partial t} = \left[B(\boldsymbol{R}) - \frac{2}{\tau_{\rm ev}} + 2\boldsymbol{U}^{(A)}(\boldsymbol{R})\cdot\nabla + \hat{D}_{ij}(\boldsymbol{R})\nabla_i\nabla_j\right]\Phi(t,\boldsymbol{R}), \qquad (7)$$

where $\boldsymbol{U}^{(A)}(\boldsymbol{R}) = (1/2)\,[\tilde{\boldsymbol{U}}(\boldsymbol{R}) - \tilde{\boldsymbol{U}}(-\boldsymbol{R})]$,

$$B(\boldsymbol{R}) \approx 2\int_0^\infty \langle b[0,\boldsymbol{\xi}(t,\boldsymbol{x}|0)]\,b[\tau,\boldsymbol{\xi}(t,\boldsymbol{x}+\boldsymbol{R}|\tau)]\rangle\,d\tau, \qquad (8)$$

$$\tilde{U}_i(\boldsymbol{R}) \approx -2\int_0^\infty \langle v_i'[0,\boldsymbol{\xi}(t,\boldsymbol{x}|0)]\,b[\tau,\boldsymbol{\xi}(t,\boldsymbol{x}+\boldsymbol{R}|\tau)]\rangle\,d\tau, \qquad (9)$$

$$\hat{D}_{ij} = 2D_m\delta_{ij} + D_{ij}^{T}(0) - D_{ij}^{T}(\boldsymbol{R}), \qquad (10)$$

$$D^{T}_{ij}(\mathbf{R}) \approx 2\int_0^\infty \langle v'_i[0,\boldsymbol{\xi}(t,\mathbf{x}|0)]\, v'_j[\tau,\boldsymbol{\xi}(t,\mathbf{x}+\mathbf{R}|\tau)]\rangle \, d\tau. \tag{11}$$

Equation (7) is written in the frame moving with the mean droplet velocity. The function $B(\mathbf{R})$ is determined by the compressibility of the droplet velocity field, $b = \operatorname{div} \mathbf{v}'$. The vector $\tilde{\mathbf{U}}(\mathbf{R})$ determines a scale-dependent drift velocity which describes transport of fluctuations of droplet number density from smaller scales to larger scales. The tensor of the scale-dependent turbulent diffusion $D^{T}_{ij}(\mathbf{R})$ tends to the tensor of the molecular (Brownian) diffusion at very small scales, while in the vicinity of the integral turbulent scale it coincides with the tensor of turbulent diffusion. Other variables in Eqs. (7)–(11) are defined as follows: δ_{ij} is the Kronecker tensor, the Wiener trajectory $\boldsymbol{\xi}(t,\mathbf{x}|s)$ in the expressions for the turbulent diffusion tensor $D^{T}_{ij}(\mathbf{R})$ and other transport coefficients is $\boldsymbol{\xi}(t,\mathbf{x}|s) = \mathbf{x} - \int_s^t \mathbf{v}[\tau,\boldsymbol{\xi}(t,\mathbf{x}|\tau)]\, d\tau + \sqrt{2D_m}\, \mathbf{w}(t-s)$, and $\langle \ldots \rangle$ denotes averaging over the statistics of turbulent velocity field and the Wiener random process $\mathbf{w}(t)$ that describes the Brownian motion. The second term in the right-hand side of Eq. (7) describes the effect of droplets evaporation.

The exponential growth of the correlation function of the droplet number density fluctuations, $\Phi(t,\mathbf{R})$, due to the tangling clustering instability, is determined by the first term, $B(\mathbf{R})\,\Phi(t,\mathbf{R})$, in the right-hand side of Eq. (7), which is the only positive one. To estimate the function $B(\mathbf{R})$ we take into account the equation of state of an ideal gas that yields: $p'/P = \rho'/\rho + \theta/T + O(\rho'\theta/\rho T)$, where ρ, T, P and ρ', θ, p' are the mean and fluctuations of the fluid density, temperature, and pressure, respectively. For small Stokes numbers, $\nabla\cdot \mathbf{v}' \approx (\tau_{\rm st}/\rho)\, \nabla^2 p' + O(\mathrm{St}^2)$, we obtain

$$\begin{aligned} B(\mathbf{R}) &\approx \frac{2\tau_{\rm st}^2}{\rho^2}\, \langle \tau[\nabla^2 p'(\mathbf{x})]\,[\nabla^2 p'(\mathbf{y})]\rangle \\ &\approx \frac{2\tau_{\rm st}^2}{\rho^2}\, \frac{P^2}{T^2}\, \langle \tau[\nabla^2\theta(\mathbf{x})]\,[\nabla^2\theta(\mathbf{y})]\rangle \end{aligned} \tag{12}$$

(see the Appendix), where τ is the turbulent time. In $\mathbf{k}$ space the correlation function $\langle \tau[\nabla^2\theta(\mathbf{x})]\,[\nabla^2\theta(\mathbf{y})]\rangle = \int \tilde{\tau}(k)\, k^4\, \langle \theta(\mathbf{k})\,\theta(-\mathbf{k})\rangle \exp(i\mathbf{k}\cdot\mathbf{R})\, d\mathbf{k}$. Taking into account that the correlation function of temperature fluctuations $\langle \theta(\mathbf{k})\,\theta(-\mathbf{k})\rangle = \langle\theta^2\rangle \tilde{E}_\theta(k)/4\pi k^2$, and integrating in $\mathbf{k}$ space, we obtain:

$$B(\mathbf{R}) \approx \frac{2\,\tau_{\rm st}^2\, c_s^4}{3\,\nu} \left(\frac{\nabla T}{T}\right)^2 \mathrm{Re}, \tag{13}$$

where c_s is the sound speed, $\tilde{E}_\theta(k) = (2/3)\, k_0^{-1}\, (k/k_0)^{-5/3}$ is the spectrum function of the temperature fluctuations for $k_0 \leqslant k \leqslant \ell_\eta^{-1}$, with $k_0 = \ell_0^{-1}$ and $\tilde{\tau}(k) = 2\tau_0\, (k/k_0)^{-2/3}$. To determine $\langle\theta^2\rangle = 2E_\theta$ we used the budget equation for the temperature fluctuations: $DE_\theta/Dt + \operatorname{div} \mathbf{\Phi}_\theta = -(\mathbf{F}\cdot\nabla)T - \varepsilon_\theta$, that for homogeneous turbulence in a steady state yields: $\langle\theta^2\rangle = -2\,\tau_0\, (\mathbf{F}\cdot\nabla)T = (2/3)(\ell_0 \nabla T)^2$, where $F_i = \langle u'_i \theta\rangle = -D_T^{(\theta)} \nabla_i T$ is the turbulent heat flux, $D_T^{(\theta)} = u_0 \ell_0/3$ is the coefficient of the turbulent diffusion of the temperature fluctuations, and the dissipation rate of E_θ is $\varepsilon_\theta = \langle\theta^2\rangle/2\tau_0$. Equation (13) implies that the correlation function $B(\mathbf{R})$ vanishes when the Reynolds number tends to zero. The effect exists only in the presence of developed turbulence.

In a nonstratified turbulence ($\nabla T = 0$), the function $B(\mathbf{R}) = 20\sigma_v/\tau_\eta(1+\sigma_v)$, where $\sigma_v \equiv \langle(\nabla\cdot\mathbf{v}')^2\rangle/\langle(\nabla\times\mathbf{v}')^2\rangle$ is the degree of compressibility of the particle velocity field. For small Stokes numbers, $\sigma_v \approx (8/3)\mathrm{St}^2$, so $B(\mathbf{R}) = 160\,\mathrm{St}^2/3\tau_\eta$, where we took into account that for a Gaussian velocity field: $\langle(\nabla\cdot\mathbf{v})^2\rangle = (80/3\tau_\eta^2)\,\mathrm{St}^2$ and $\langle(\nabla\times\mathbf{v})^2\rangle = 10/\tau_\eta^2$ (for details see Ref. [12]). On the other hand, for stratified turbulence ($\nabla T \neq 0$) and small Stokes number,

$$B(\mathbf{R}) \approx \frac{2\,\tau_{\rm st}^2\, c_s^4}{3\,\nu}\left(\frac{\nabla T}{T}\right)^2 \mathrm{Re} = \frac{160\,\tilde{\mathrm{St}}^2}{3\tau_\eta} = \frac{20\tilde{\sigma}_{\rm v}}{\tau_\eta}, \tag{14}$$

where $\tilde{\mathrm{St}} = \mathrm{St}\,\Gamma$, $\tilde{\sigma}_v \approx (8/3)\tilde{\mathrm{St}}^2$,

$$\Gamma(\mathrm{Re}, L_{\rm eff}/L_T) = \mathrm{Re}^{1/2}\left(\frac{L_{\rm eff}\,\nabla T}{T}\right), \tag{15}$$

and variables with tilde symbols correspond to those for stratified turbulence. Here $L_{\rm eff} = c_s^2 \tau_\eta^{3/2}/9\nu^{1/2}$ is an effective length scale, and $L_T = T/|\nabla T|$ is the characteristic scale of the mean temperature variations.

In the general case that includes both the tangling clustering instability and the inertial clustering instability, the parameter Γ can be written in the following form:

$$\Gamma(\mathrm{Re}, L_{\rm eff}/L_T) = \left[1 + \mathrm{Re}\left(\frac{L_{\rm eff}\,\nabla T}{T}\right)^2\right]^{1/2}, \tag{16}$$

where the inertial clustering instability corresponds to the case of $\Gamma = 1$. For typical parameters of atmospheric turbulence: (i) $\mathrm{Re} = 10^7$ ($u_0 = 1$ m/s, $\ell_0 = 100$ m) and the mean temperature gradient, $|\nabla T| = (0.3-1)$ K / 100 m, the effective length $L_{\rm eff} = 23$ km, the dimensionless parameter $\Gamma = (1-2)\times 10^3$; (ii) $\mathrm{Re} = 10^6$ ($u_0 = 0.3$ m/s, $\ell_0 = 30$ m) and the mean temperature gradient, $|\nabla T| = (0.3-1)$ K / 100 m, the effective length $L_{\rm eff} = 130$ km, the dimensionless parameter $\Gamma = (1-4)\times 10^3$.

When the Stokes number is not small, the degree of compressibility is given by

$$\sigma_{\rm v} = \frac{(8/3)\mathrm{St}^2}{1+\mathrm{St}^2} \tag{17}$$

(for details see Ref. [13]). Since for the stratified turbulence $B(\mathbf{R}) = 20\tilde{\sigma}_v/\tau_\eta(1+\tilde{\sigma}_v)$, and $\tilde{\sigma}_v = (8/3)\tilde{\mathrm{St}}^2/(1+\tilde{\mathrm{St}}^2)$, the function $B(\mathbf{R})$ for the stratified turbulence and for arbitrary Stokes numbers reads:

$$B(\mathbf{R}) = \frac{160\,\mathrm{St}^2\,\Gamma^2}{\tau_\eta(3 + 11\,\mathrm{St}^2\,\Gamma^2)}. \tag{18}$$

For $\Gamma = 1$ Eq. (18) describes the inertial clustering. When the diameter of the droplet $d \approx 1.7\,\mu$m, $\mathrm{St}^2\,\Gamma^2 \approx 3/11$. This implies that when the diameter of the droplets is much larger than $1.7\,\mu$m, the parameter $\mathrm{St}^2\,\Gamma^2 \gg 3/11$, and the function $B(\mathbf{R}) \sim 160/11\tau_\eta$ is independent of the Stokes number and the size of droplets. As can be seen from Eq. (18) the effect of tangling clustering is much stronger than the inertial clustering only for droplets smaller than $20\,\mu$m. Remarkably, the inertial clustering instability can be excited only if the size of droplets is larger than $20\,\mu$m (see Ref. [12]). Analysis of the solution of Eq. (7) for the two-point second-order correlation function, $\Phi(t,\boldsymbol{R})$, performed in Sec. V in Ref. [30], shows that the ratio of the minimum and maximum of the pair correlation function reads:

$$\frac{\Phi_{\min}}{\Phi_{\max}} = -\frac{\pi}{e\,\lambda}\left(\frac{\mathrm{Sc}^{-\lambda/2}}{\ln \mathrm{Sc}}\right), \tag{19}$$

where $\mathrm{Sc} = \nu/D_m$ is the Schmidt number and the parameter $\lambda(\tilde{\sigma}_v) = (20\tilde{\sigma}_v + 1)/4(\tilde{\sigma}_v + 1)$ in Eq. (19) depends on the degree of compressibility of the particle velocity field, $\tilde{\sigma}_v$. For typical parameters of atmospheric turbulence, parameter λ varies in the range from 0.5 to 2.5.

As follows from Eq. (18), the temperature fluctuations, which are caused by the tangling of the mean temperature gradient, ∇T, by the fluid velocity fluctuations $\boldsymbol{u}'$, strongly contribute to the function $B(\boldsymbol{R})$ and the growth rate of the tangling clustering instability in the temperature-stratified turbulence. The mechanism of coupling related to the tangling of the gradient of the mean temperature gradient is quite robust. The tangling is not sensitive to the exponent of the energy spectrum of the background turbulence. Anisotropy effects do not introduce new physics in the clustering process because the main contribution to the tangling clustering instability is at the Kolmogorov (viscous) scale of turbulent motions, where turbulence can be considered as nearly isotropic, while anisotropy effects can be essential in the vicinity of the maximum scales of the turbulent motions.

Equation (16) shows that the tangling clustering instability can be much more effective than the inertial clustering instability which is excited in a nonstratified turbulence [12]. In both instabilities, the particle clustering is determined by the two-point correlation function of the Laplacian of air pressure fluctuations. However, in the case of nonstratified turbulence the pressure fluctuations are of the order of $\rho \boldsymbol{u}'^2$, while in the case of the temperature-stratified turbulence there are additional pressure fluctuations caused by temperature fluctuations, $p' \propto P(\theta/T) \propto (P/T)\ell_0|\nabla T|$, where we took into account that the root mean square of the tangling temperature fluctuations $\theta \sim \ell_0|\nabla T|$ (see Ref. [37]). Consequently, the ratio of the two-point correlation functions of the Laplacian of air pressure fluctuations in stratified and nonstratified flows is proportional to

$$\frac{B_{\rm tangling}}{B_{\rm isothermal}} \sim \left(\frac{\tilde{n} k_B T}{\rho \boldsymbol{u}^2}\right)^2 \frac{\ell_0^2}{L_T^2}, \tag{20}$$

which is a large parameter because the thermal energy density $\tilde{n} k_B T$ is much larger than the turbulent kinetic energy $\rho \boldsymbol{u}'^2$, where $\tilde{n}$ is the number density of molecules. Here we used the equation of state for the ideal gas $P = \tilde{n} k_B T$.

Due to inertia effects, droplets accumulate in the regions with increased pressure of the air flow. The effect of increased pressure fluctuations in a temperature-stratified turbulence is more pronounced in small scales because the function $B(\boldsymbol{R})$ is determined by the two-point correlation function of the Laplacian of pressure fluctuations. The tangling clustering is also enhanced by the effect of turbulent thermal diffusion [38] that causes nondiffusive streaming of particles in the direction of a heat flux and accumulation of particles in the regions with the minimum mean temperature of the air flow.

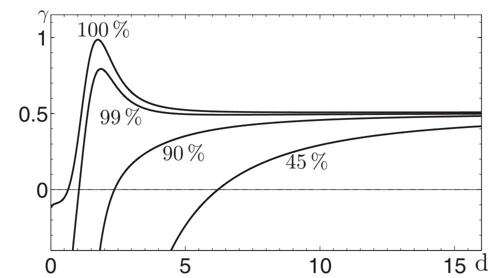

FIG. 1. Growth rate γ of the tangling clustering instability (measured in units $1/\tau_\eta$) versus the droplet diameter d (measured in μm) for $\Gamma = 10^3$ and $\mathrm{Sc} = \nu/D_m = 5 \times 10^5 d$ (μm).

Temperature fluctuations in the stratified turbulence produce pressure fluctuations and cause particle clustering due to the tangling clustering instability with the growth rate, that is, by a factor $\mathrm{Re}(L_{\rm eff}/L_T)^2$ larger than the growth rate of the inertial clustering instability [see Eq. (16)]. For large Reynolds numbers the tangling mechanism is universal and weakly dependent on the origin of turbulence.

C. Growth rate of the instability

To illustrate the tangling clustering instability we use the standard dependence of the droplet evaporation time on their diameter and the relative humidity [see Eq. (26) below]. Figure 1 shows the growth rate of the instability (measured in the inverse turbulent Kolmogorov time scale units, τ_η^{-1}) versus the droplet diameter d (measured in μm) for different values of relative humidity, ϕ, i.e., for very low humidity (45% and 90%) and for very high humidity (99% and 100%). Inspection of Fig. 1 shows that the threshold for the tangling clustering instability based on the size of the droplets is $d_{\rm th} = 0.7\ \mu$m. The instability is excited when $d > d_{\rm th}$, and there is a sharp maximum of the growth rate of the instability at $d = 1.75\ \mu$m if the relative humidity is close to saturation, 99% and 100%. This explains the fast growth of the droplets having the initial diameter of the order of 1.75 μm caused by the tangling clustering instability. For lower values of the relative humidity the threshold for the tangling clustering instability increases and the droplet growth rate sharply decreases. For $d \geqslant 5\ \mu$m and for very high humidity (99% and 100%) the growth rate of the tangling clustering instability is constant and independent of the droplet size.

The exponential growth of droplet number density inside the cluster is saturated by nonlinear effects. The droplet number density inside the cluster can be constraint by depletion of particles in the surrounding air flow caused by their accumulation inside the cluster. Another effect that inhibits the growth of the droplet number density inside the cluster is related to a strong momentum coupling of particles and turbulent air flow when the mass loading parameter $m_{\rm dr} n_{\max}/\rho \approx 0.5$.

It can be shown [30] that the maximum increase of particle number density inside the cluster, $n_{\max}/N$, caused by the first effect is

$$\frac{n_{\max}}{N} = \left(1 + \frac{e\,\lambda}{\pi}\,\mathrm{Sc}^{\lambda/2}\,\ln \mathrm{Sc}\right)^{1/2}. \tag{21}$$

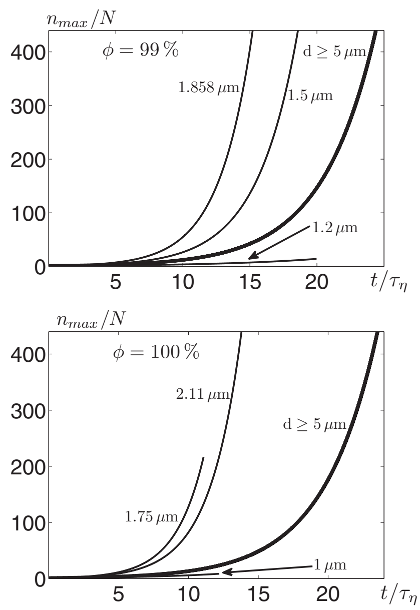

FIG. 2. The time evolution of droplet concentration $n_{\rm max}/N$ inside the cluster for droplets of different diameter for relative humidity 99% (upper panel) and 100% (bottom panel); $\Gamma = 10^3$ and $\mathrm{Sc} = 5 \times 10^5\, d$. Thick solid line corresponds to droplets with $d \geqslant 5\ \mu$m (for which the growth rate of the tangling clustering instability is independent of the droplet size).

In this analysis small yet finite molecular diffusion D_m has been taken into account. In the limit $D_m = 0$ Eq. (21) is not valid. For instance, the Schmidt number for droplets in the atmospheric flow is $\mathrm{Sc} = 5 \times 10^5\, d\ (\mu\mathrm{m})$.

Let us estimate the limitation caused by strong momentum coupling of particles and turbulent air flow. Assuming as total cloud water content $\bar{\rho}_{\rm dr} \equiv m_{\rm dr} n_{\rm max} = 1.5\ \mathrm{g/m^3}$ and taking into account that the air density in the atmosphere $\rho \approx 1.3 \times 10^3\ \mathrm{g/m^3}$, we obtain: $n_{\rm max}/N < 0.5\, \rho/\bar{\rho}_{\rm dr} \approx 470$.

Figure 2 shows the increase of droplets concentration $n_{\rm max}/N$ inside the cluster during development of the tangling clustering instability for the relative humidity 99% and 100% and for different droplet sizes. The growth rate of the instability is of the order of 10 inverse Kolmogorov time scales, where $\tau_\eta \approx 0.1$ s. In this study we consider only droplet clustering, but not aerosol dynamics. Clearly, the clustering of aerosols is similar to that of droplets for humidity of 100%, i.e., without evaporation.

Strong increase of clustering in a temperature-stratified fluid in comparison with the inertial clustering has been confirmed in laboratory experiments [32]. The experimental study of the particle clustering compared the two-point correlation functions for both inertial and tangling clustering measured with sub-Kolmogorov scale resolution. The experimental parameters were the rms velocity $u_0 = 12$ cm/s, the integral (maximum) scale of turbulence $\ell_0 = 3.2$ cm, the Reynolds numbers $\mathrm{Re} = 250$, the Kolmogorov length scale $\ell_\eta = 510\ \mu$m, and the Kolmogorov time scale $\tau_\eta = 1.7 \times 10^{-2}$ s. The Stokes time for the particles with the diameter $d = 10\ \mu$m is $\tau_{\rm st} = 10^{-3}$ s, the Stokes number $\mathrm{St} = 5.9 \times 10^{-2}$, the coefficient of molecular diffusion $D_m = 1.4 \times 10^{-8}\ \mathrm{cm^2/s}$, and the Peclet number $\mathrm{Pe} = u_0\, \ell_0/D_m = 3 \times 10^9$. These experiments demonstrated that the two-point correlation function of the particle number density fluctuations for the tangling clustering in temperature-stratified turbulence is by one order of magnitude larger than that for the inertial clustering in isothermal turbulence [32]. This is consistent with the efficiency of the tangling clustering being proportional to $\mathrm{Re}^{1/2}$ [see Eq. (16)]. In these laboratory experiments $\mathrm{Re}^{1/2} \sim 15$. Since in the atmospheric turbulence the Reynolds number is 10^7 ($\mathrm{Re}^{1/2} \sim 3 \times 10^3$) it is plausible to suggest that for atmospheric conditions the effect of the tangling clustering will be more pronounced.

III. DETECTION OF DROPLET CLUSTERING IN ATMOSPHERIC CLOUD MEASUREMENTS

In this section we present a short discussion of the existing cloud measurements and their relation to the droplet clustering. Aircraft mounted with forward-scattering spectrometer probe [39] was used for study of 1-cm droplet concentrations in cumulus clouds. In these experiments over 50 cloud passes have been done. The statistical analysis in Ref. [39] has shown significant deviations from the Poisson distribution, which characterizes a random homogeneous spatial distribution of the droplets. These findings were interpreted in Ref. [39] as appearance of small-scale (about 1-cm) droplet clusters in cumulus clouds.

The droplet clusters were detected in Ref. [40] by analyzing the measurements obtained *in situ* in 57 clouds by use of the fast forward-scattering spectrometer probe (FSSP). This finding is direct evidence of the turbulence-inertia impact on droplet motion in clouds. The dissipation rate of the turbulent kinetic energy in clouds was varied in the atmospheric measurements [40] from 10^{-4} to $2.3 \times 10^{-2}\ \mathrm{m^2\ s^{-3}}$. The rms of small-scale droplet concentration fluctuations was estimated to be about 31% of the mean values of droplet concentration both over the whole cloud and in a more homogeneous adiabatic core. The power spectrum shows that fluctuations with spatial scales within the 0.5- to 5-cm range contain over 80% of the energy of small-scale fluctuations [40]. An increase in turbulence intensity and droplet inertia result in an increase of the droplet concentration fluctuations.

In other experiments [41] the droplet positions have been measured with the Meteo-France fast forward-scattering spectrometer probe. The cloud droplet data were collected during a single traverse by the Meteo-France Merlin IV research aircraft through a cumulus cloud encountered during the Small Cumulus Microphysics Study. The energy dissipation rate was of the order of $10^{-4}\ \mathrm{m^2\ s^{-3}}$. The collected data in Ref. [41] reveal droplet clustering even in cumulus cloud cores free of entrained ambient air. The pair correlation function was obtained in Ref. [41] for droplets in a high-Reynolds-number turbulent flow. The super-Poissonian variances which were detected in these homogeneous core data were viewed in Ref. [41] as conclusive evidence of clustering. It was shown in Ref. [42], by using the correlation-fluctuation theorem and the Wiener-Khinchin theorem, that the pair-correlation function is ideal for quantifying droplet clustering because it contains no scale memory and because of its quantitative link to the Poisson process.

Simultaneous observations of cloud droplet spatial statistics, cloud droplet size distribution, and cloud turbulence were made in Ref. [43] during several cloud passages, including cumulus clouds and a stratus cloud. The measurements were conducted using the Airborne Cloud-Turbulence Observation System (ACTOS), which was suspended from a tethered balloon. The ACTOS instrumental payload was equipped with sensors to measure the three-dimensional wind velocity, static air temperature, and humidity with a sampling frequency of at least 100 Hz. The wind velocity was measured by an ultrasonic anemometer. Cloud droplet number density and droplet size distribution were obtained from measurements with the M-Fast-FSSP, which records sizes and arrival times of individual droplets. The primary finding of the study in Ref. [43], by determining the droplet pair correlation function (with the spatial resolution about 100–200 μm), is the indication of the droplet clustering even for small Stokes numbers (smaller than 10^{-2}) and also in weakly turbulent clouds (with the dissipation rate of the turbulent kinetic energy that is smaller than 10^{-2} m^2 s^{-3}). For three analyzed cases, two horizontal passages through cumulus clouds and vertical profiles through a stratus cloud, the regions where droplets are clustered at sub-cm scales, were found in Ref. [43].

All these studies for the most part show very modest clustering at Kolmogorov separations and below. Note, however, that the FSSP measures droplets along a narrow almost 1D horizontal path through a cloud volume, which means that a long sample is necessary to construct a reasonable spectrum [2]. The interpretation of the results remains controversial because deviations from Poisson distributions could be possible due to instrumental artifacts and the necessarily limited samples that are obtained from aircraft measurements, which inevitably compromise the assumption of the statistical homogeneity of the sample [2]. Unfortunately, the detailed measurements during all these atmospheric cloud experiments of the spatial temperature distributions and of the vertical and horizontal heat fluxes in clouds have not been presented in the papers discussing the droplet clustering. Consequently, we cannot make any conclusions about tangling clustering in these experiments.

It must be emphasized that the pair correlation function $\Phi(\boldsymbol{R})$ for the clustered droplet population measured in Ref. [43] (see Fig. 1 in Ref. [43]) agrees with the pair correlation function determined analytically in our previous study (see Eqs. (43) and (47) in Ref. [30]). The discrepancy occurs only in the scales smaller than a Kolmogorov scale (that is, $\ell_\eta = 2$ mm in Ref. [43]). Our theory predicts that the pair correlation function vanishes in the vicinity of ℓ_η, in agreement with the atmospheric experiments (reported in Ref. [43]), as well as with our laboratory experiments (see Ref. [32]). However, the pair correlation function $\Phi(\boldsymbol{R})$ according to our theory (see Ref. [30]) sharply increases at smaller scales. The ratio of the minimum and maximum of the pair correlation function, $\Phi_{\rm min}/\Phi_{\rm max}$, is given by Eq. (19) of the present paper (or Eq. (62) in Ref. [30]). Using the value of $\Phi_{\rm min} = -0.05$ measured in Ref. [43] and the parameters of turbulence and droplets for the atmospheric experiments in Ref. [43] we find that ${\rm Sc} \equiv {\rm Pe}/{\rm Re} = 3 \times 10^4$ and the ratio $\Phi_{\rm max}^{1/2}/N$ is of the order of 500, where Pe is the droplet Peclet number. This value of the ratio $\Phi_{\rm max}^{1/2}/N$ agrees with the estimated value 470 obtained in Ref. [30]. To determine the pair correlation function in the scales much smaller than the Kolmogorov scale, the spatial resolution of the atmospheric measurements reported in Ref. [43] should be improved by a factor of 10 at least. Conducting measurements in these scales may require us to abandon the Taylor hypothesis and to employ the particle image velocimetry or holographic techniques. In this case the radial distribution function (RDF), $G(\mathbf{R}) = \langle n(t,\mathbf{x}) n(t,\mathbf{y})\rangle / N(t,\mathbf{x}) N(t,\mathbf{y})$, can be determined from two-dimensional images of a field of M droplets by binning the droplet pairs according to their separation distance, so the function $G(\mathbf{R})$ is determined as follows:

$$G(\mathbf{R}) \approx \frac{N_{\Delta S}^{(p)}/\Delta S}{N_S^{(p)}/S}, \tag{22}$$

where $\Delta S = \pi[(R+\Delta R/2)^2 - (R-\Delta R/2)^2]$ is the area of the annular domain located between $R \pm \Delta R/2$ and S is the area of the part of the image with the radius $R_{\rm max}$ that is used in data processing in order to exclude the edge effects. The measured radial distribution function allows us to determine the two-point correlation function of the droplet number density, $\Phi(t,\mathbf{R}) = N^2\,[G(t,\mathbf{R}) - 1]$.

In order to attain a high spatial resolution, the following method should be used: (i) to determine the response function for the charge-coupled device (CCD) camera by analyzing the light intensity distribution in the image for single droplet located at the center of the pixel in the form of the Gaussian distribution, (ii) segmentation of the image using a threshold technique, and (iii) identification of droplet locations in the segments by least-squares fitting of the recorded light intensity distribution and the light intensity distribution caused by superposition of the Gaussian distributions at the droplet locations (for details see Ref. [32]).

To detect the tangling clustering in the atmospheric clouds, the measurements of the spatial temperature distributions in clouds, as well as the fluid velocity measurements, should be conducted in addition to the measurements of RDF of droplets. In particular, it is important to measure the vertical and horizontal heat fluxes, $\langle \mathbf{u}\,\theta\rangle$, and two-point correlation functions of the temperature fluctuations, $\langle \theta(\mathbf{x})\,\theta(\mathbf{y})\rangle$, in clouds. This allows us to determine the rate of tangling clustering $B(\mathbf{R})$ [see Eqs. (12) and (18)]. In addition, measurements of two-point noninstantaneous correlation functions of fluid velocity allow us to determine the integral scale of turbulence and turbulent time scales. Measurements of turbulent fluxes of droplets $\langle \mathbf{u}\,n'\rangle$ in combination with the measurements of spatial distributions of droplets allow us to determine the turbulent diffusion coefficients of droplets.

IV. COLLISION KERNEL AND DROPLET COAGULATION

In this section we consider droplet coagulation and apply the theory of the tangling clustering instability to explain acceleration of raindrops formation in warm clouds. The warm clouds often exist in the region of atmospheric turbulent convection with coherent structures (cloud "cells" in shear-free convection and cloud "streets" in sheared convection, see, e.g., Ref. [44,45]). The vertical large-scale temperature gradient is small inside the large-scale circulation (coherent structures) in a small-scale turbulent convection. However, the horizontal large-scale temperature gradient inside the circulations is not small. Atmospheric observations showed that this gradient is about 1 K/100 m [46]. Similar results were reported in laboratory experiments where the horizontal large-scale temperature gradient inside the large-scale circulation was 0.6 K/cm, while the vertical large-scale temperature gradient was 0.05 K/cm [47]. This magnitude of the horizontal temperature gradient is sufficient for the generation of strong temperature fluctuations in the stratified turbulence by use of the tangling mechanism.

The initial stage of cloud droplets formation involves condensation of water vapor on CCN and formation of small micron-sized droplets. In the present study we show that the tangling clustering instability strongly enhances the growth rate of cloud droplets at both stages: at the first stage when droplets grow from the micron size to 10-μm droplets and at the next stage from 10- to 50-μm radius droplets.

A. Smoluchowski coagulation equation

Subsequent evolution and growth of small droplets due to collision-coalescence depend on the interplay between their collision time and evaporation time, in particular because of water vapor depletion. The collision time of small droplets can be determined using the Smoluchowski coagulation equation (see, e.g., Ref. [48], chap. 13):

$$\frac{\partial \tilde{n}(d)}{\partial t} + \mathrm{div}(\tilde{n}\, \boldsymbol{v}) - D_m \Delta \tilde{n} + \frac{\tilde{n}}{\tau_{\rm ev}} = \frac{1}{2}\int_0^d K(\hat{d},x)\, \tilde{n}(\hat{d})\, \tilde{n}(x)\, dx - \int_0^\infty K(d,x)\, \tilde{n}(x)\, \tilde{n}(d)\, dx, \qquad (23)$$

where $\hat{d} = (d^3 - x^3)^{1/3}$, $\tilde{n}(d)$ is the droplet size distribution, $n = \int \tilde{n}(x)\, dx$ is number density of droplets, and $K(d,x)$ is the coagulation kernel that describes coagulation rate of droplets of the diameter d and droplets of the diameter x. In the present study we use the coagulation kernel $K(d,x)$ as a sum of the Brownian coagulation kernel (see Table 13.1, p. 600 in Ref. [48]) and the gravitational coagulation kernel (see Eq. (13.A.4), p. 615 in Ref. [48]).

Averaging Eq. (23) over the statistics of particle turbulent velocity field, estimating integrals in Eq. (23), using the mean-value theorem, and taking into account that $\langle \tilde{n}(d)\, \tilde{n}(d_1)\rangle$ is calculated in the same point, so $\langle \tilde{n}(d)\, \tilde{n}(d_1)\rangle \leqslant \tilde{n}_{\rm max}(d)\, \tilde{n}_{\rm max}(d_1) = C(d,d_1)\, \tilde{N}(d)\, \tilde{N}(d_1)$, we obtain the following equation for the mean droplet size distribution $\tilde{N}(d)$:

$$\frac{\partial \tilde{N}(d)}{\partial t} + \mathrm{div}(\tilde{N}\, \boldsymbol{V}_{\rm dr} + \langle \tilde{n}'\, \boldsymbol{u}\rangle) = -\frac{\tilde{N}}{\tau_{\rm ev}(d)} - \frac{\tilde{N}}{\tau_{\rm eff}^{\rm st}(d)} + D_T\, \Delta \tilde{N}, \qquad (24)$$

where $C(d,d_1) = \tilde{n}_{\rm max}(d)\, \tilde{n}_{\rm max}(d_1)/\tilde{N}(d)\, \tilde{N}(d_1)$, $D_T(d)$ is the turbulent diffusion coefficient, and

$$\tau_{\rm eff}^{\rm st}(d) = \frac{1}{\tilde{N}(d)\, K(d,d_1)\, C(d,d_1)} > \frac{1}{\tilde{N}(d)\, K(d,d_1)} \left[\frac{\tilde{n}_{\rm max}(d)}{\tilde{N}(d)}\right]^{-2}. \qquad (25)$$

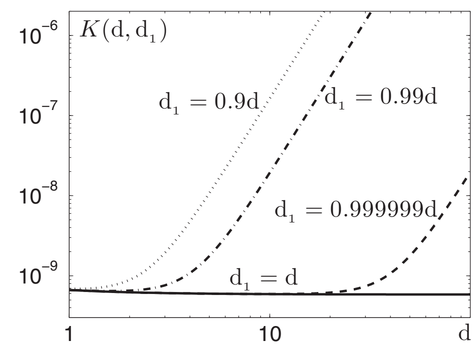

FIG. 3. Sum of Brownian and gravitational coagulation kernels versus the droplet diameter d in microns for two droplets having different diameters: $d = 0.9d_1$ (dotted line), $d = 0.99d_1$ (dashed-dotted line), and $d - d_1 = 10^{-6}d$ (dashed line). The solid line is the Brownian coagulation kernel $K(d,d_1)$ [measured in cm^3/s] for two droplets having equal diameters $d = d_1$. The diameter d of droplets is measured in μm.

Notably, the collision term $\tilde{N}(d)/\tau_{\rm eff}^{\rm st}(d)$ in Eq. (24) is similar to the droplet evaporation term. The coefficient of molecular diffusion of droplets having the diameter d in the atmosphere is $D_m = 2 \times 10^{-7}/\, d(\mu\mathrm{m})\, \mathrm{cm}^2\, \mathrm{s}^{-1}$, while the turbulent diffusion coefficient $D_T = u_0 \ell_0/3 = 3 \times 10^5\, \mathrm{cm}^2\, \mathrm{s}^{-1}$, where turbulent velocity u_0 at the integral turbulent scale $\ell_0 = 100$ m is $u_0 = 1$ m/s. Therefore, the coefficient of molecular diffusion of droplets is much smaller than the turbulent diffusion coefficient.

B. Effective collision-coalescence time

Now we can estimate the droplet collision time and compare it with the evaporation time of droplets having different sizes. The most interesting case is the growth of droplets when the relative humidity is only slightly less 100% and the evaporation of droplets competes with their coagulation. Figure 3 shows the numerical values of the sum of the Brownian and gravitational coagulation kernels versus droplet diameter d when droplets have the same or different sizes [48]. Inspection of Fig. 3 shows that the collision kernel varies slightly when $d < 2\,\mu$m, and it increases by one order of magnitude for $d = 5\,\mu$m, while for $d > 5\,\mu$m the collision kernel can increase by three orders of magnitude depending on the difference in size of colliding droplets (d and d_1). However, the effect of this increase on the droplet collision rate is much smaller than the increase of droplet collision rate due to the increase of the droplet number density caused by the tangling clustering instability that is up to five orders of magnitude.

Dynamics of the raindrops evolution and their growth depend on the interplay between the characteristic times of droplet collisions resulting in droplet coagulation and the time of droplet evaporation. The characteristic times of vapor diffusion and thermal relaxation in the gaseous phase in the vicinity of a droplet can be estimated as $\tau_{\rm dif} \propto d^2/D_v$ and $\tau_{\rm th} \propto d^2/\chi$, where $D_{\rm v} = 0.216\, \mathrm{cm}^2\, \mathrm{s}^{-1}$ is the coefficient of binary diffusion of water vapor in air and $\chi = 0.185\, \mathrm{cm}^2\, \mathrm{s}^{-1}$ is the thermal diffusivity of air [48]. Since these characteristic times are much smaller than the time of droplet evaporation or growth, the evaporation or growth of cloud droplets is

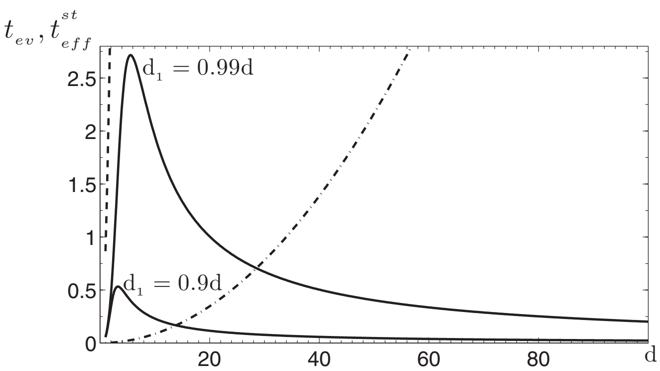

FIG. 4. Evaporation times versus droplet diameter for relative humidity $\phi = 99\%$ (dashed-dotted line) and $\phi = 99.99\%$ (dashed line) and effective collision-coalescence time (solid lines for different $d - d_1$). The diameter d of droplets is measured in μm and time is measured in minutes.

determined by stationary vapor diffusion. In this case, the characteristic time of the decrease of droplet radius due to evaporation can be estimated using the coupled analytical model of the evaporation or growth rates of droplets (see Ref. [36]). For the ambient air temperature $T_a = 274$ K, this model yields the following expression for the evaporation time:

$$\tau_{\rm ev} = 0.5 \times 10^{-3} \frac{d^2}{1-\phi}, \tag{26}$$

where the droplet diameter is measured in microns and time is given in seconds. The calculated evaporation times versus droplet radius for relative humidity $\phi = 99\%$ and $\phi = 99.99\%$ together with the effective collision-coalescence time within the cluster are shown in Fig. 4. To determine the effective collision-coalescence time we have assumed that a total cloud water content of mean droplets mass density is about $\bar{\rho}_{\rm dr} = 1.5\,{\rm g/m^3}$, which corresponds to the typical mean number density of 10 μm droplets, $N \approx 2\,{\rm cm^{-3}}$, while for 2 μm droplets it is about $N \approx 2 \times 10^2\,{\rm cm^{-3}}$.

In the absence of tangling clustering instability, for the ambient number density of the micron-size droplets having the mean number density $N \approx 10^2\,{\rm cm^{-3}}$, the collision-coalescence time is of the order of $\tau^{\rm st}_{\rm eff}(d = 2\,\mu{\rm m}) \approx (\tilde{N}\,K)^{-1} \approx 10^7$ s, and for droplets with diameter $d = 10\,\mu$m and the mean number density $N(d = 10\,\mu{\rm m}) \approx 1\,{\rm cm^{-3}}$, the collision-coalescence time is $\tau^{\rm st}_{\rm eff}(d = 10\,\mu{\rm m}) > 10^7$ s. These values are too large to account for the collision-coalescence growth of cloud droplets since the droplet evaporation time is much less than their collision time. The latter conclusion implies that small micron-size and submicron-size droplets are either in equilibrium or grow very slowly due to condensation of supersaturated water vapor. In these calculations we have taken into account kinetic corrections to submicron-size droplet evaporation time using the flux-matching approach suggested in Ref. [49].

The situation drastically changes in the presence of the tangling clustering instability. In this case the droplet collision time inside the clusters, which are formed due to the tangling clustering instability, decreases by the large factor, $[n_{\rm max}/N]^2 \sim 10^5$. Indeed, the number density of droplets inside the cluster sharply increases and their effective collision time dramatically decreases:

$$\tau^{\rm st}_{\rm eff} = \frac{1}{\tilde{N}(d)\,K(d,d_1)} \left(\frac{n_{\rm max}}{N}\right)^{-2}. \tag{27}$$

Using the numerical values of the coagulation kernel showed in Fig. 3 we can estimate the effective collision-coalescence time inside the cluster. The equilibrium between the effective droplet collision-coalescence and droplet evaporation depends on the value of the relative humidity ϕ and the temperature of the ambient air. The calculated effective collision times inside the cluster for two typical values of the relative humidity for $T = 274$ K versus the droplet diameter are shown by solid lines in Fig. 4.

Using data shown in Fig. 4, we estimate the time of growth of droplets by cascade of successive collisions of droplets having close diameters (with diameters ratios $d_1/d = 1.1$ or $d_1/d = 1.01$). In the calculations we take into account that after each collision droplet the diameter increases and the effective droplet collision time changes nonmonotonically, as shown in Fig. 4. For $d_1/d = 1.1$ the time of droplet size growth diameter from 1 to 10 μm is about 3 min, while for $d_1/d = 1.01$ this time is approximately 11 min. The time required for further droplet size growth from 10-μm to 50- to 60-μm diameter droplets is about 1 min for $d_1/d = 1.1$ and 5.5 min for the colliding droplet diameter ratio $d_1/d = 1.01$. It should be noted that the real droplet size growth time can be shorter due to direct enhancement of the droplet collision kernel by turbulence (see Ref. [1] and references therein). Since the droplet collisional growth time is smaller for droplets with larger diameters ratios, the estimated droplet growth time can be considered a fairly reasonable estimate of the time required for droplet growth. The total time required for collisional growth of droplets having a diameter of 1 μm to droplets having a diameter of 50 μm is of the order of 15 min, which is close to the observed 15 to 20 min required for formation of rain droplets.

V. CONCLUSIONS

A new effect of the tangling clustering instability of small droplets in a turbulent temperature-stratified atmosphere results in the formation of clusters with drastically increased droplet number density and, correspondingly, a sharply increased rate of their collision-coalescence. Without the tangling clustering instability, the droplets' collision-coalescence time is much larger than the characteristic time of droplet evaporation. Consequently, in the absence of tangling clustering instability droplets do not grow due to collision-coalescence, and rain droplets are not formed. On the contrary, in the presence of tangling clustering instability the effective collision-coalescence time inside the clusters strongly decreases by the factor $[n_{\rm max}/N]^2 \sim 10^5$. As a result, droplets within the cluster coalesce and grow, forming large rain droplets. The growth time of droplets from the initial size of 1 μm to the size of about 50 μm is 15–20 min.

In summary, we can conclude that the effect of the tangling clustering instability provides a convincing explanation of the observed fast growth of cloud droplets.

ACKNOWLEDGMENTS

This work was supported by the Israel Science Foundation governed by the Israeli Academy of Sciences (Grant No. 1037/11), the Research Council of Norway under the FRINATEK (Grant No. 231444), the Academy of Finland (Grant No. 280700), Russian Science Foundation (Grant No. 15-17-20009), and grant from the Russian Ministry of Science and Education (Program 1.5/XX, Contract No. 8648). N.K. and I.R. thank NORDITA for hospitality and support during their visits. Part of this work was completed while participating at the NORDITA program on "Dynamics of Particles in Flows: Fundamentals and Applications."

APPENDIX: DERIVATION OF THE FUNCTION $B(\boldsymbol{R})$

Let us determine the functions $B(\boldsymbol{R})$:

$$B(\boldsymbol{R}) \approx \frac{2\tau_{\rm st}^2}{\rho^2} \langle \tau [\nabla^2 p'(\boldsymbol{x})]\, \nabla^2 p'(\boldsymbol{y})\rangle \approx \frac{2\tau_{\rm st}^2}{\rho^2} \left[\frac{P^2}{T^2} \langle \tau [\nabla^2 \theta(\boldsymbol{x})]\, \nabla^2 \theta(\boldsymbol{y})\rangle + \frac{P^2}{\rho^2} \langle \tau [\nabla^2 \rho'(\boldsymbol{x})]\, \nabla^2 \rho'(\boldsymbol{y})\rangle + \frac{P^2}{\rho\, T} (\langle \tau [\nabla^2 \rho'(\boldsymbol{x})]\, \nabla^2 \theta(\boldsymbol{y})\rangle + \langle \tau [\nabla^2 \theta(\boldsymbol{x})]\, \nabla^2 \rho'(\boldsymbol{y})\rangle) \right], \tag{A1}$$

where $\nabla^2 p'(\boldsymbol{x}) = [\nabla^{(x)}]^2 p'(\boldsymbol{x})$ and ρ' are the fluid density fluctuations. In derivation of this equation we used the relationship

$$\frac{p'}{P} = \frac{\rho'}{\rho} + \frac{\theta}{T} + O(\rho'\,\theta) \tag{A2}$$

that follows from the equation of state for an ideal gas. We also take into account that characteristic spatial scales for fluctuations of fluid pressure, temperature, and density are much less than those for the mean fields.

In stratified turbulence with turbulent heat flux, the correlation function $\langle \theta(\boldsymbol{x}) \theta(\boldsymbol{y})\rangle$ is much larger than the correlation functions of density-density fluctuations or density-temperature fluctuations. Indeed, the correlation function $\langle [\nabla^2 \theta(\boldsymbol{x})]\, \nabla^2 \theta(\boldsymbol{y})\rangle$ is caused by the turbulent heat flux, i.e., $\langle \theta(\boldsymbol{x})\, \theta(\boldsymbol{y})\rangle \propto -\tau_0 \, \langle u_i(\boldsymbol{x})\, \theta(\boldsymbol{y})\rangle\, (\nabla_i T)$, where τ_0 is the characteristic turbulent time. On the other hand, the correlation functions of density-density fluctuations or density-temperature fluctuations are nearly independent of the turbulent heat flux, and they are proportional to the mass flux $\langle \boldsymbol{u}(\boldsymbol{x})\, \rho'(\boldsymbol{y})\rangle$, which is very small for low-Mach-number flows. In particular, the temperature fluctuations can be estimated as $\theta \propto -\tau_0\, u_i\, \nabla_i T$. Consequently, the temperature-density correlator can be estimated as $\langle \theta(\boldsymbol{x})\, \rho'(\boldsymbol{y})\rangle \propto -\tau_0 \, \langle u_i(\boldsymbol{x})\, \rho'(\boldsymbol{y})\rangle\, (\nabla_i T)$. The density fluctuations are determined by the continuity equation:

$$\frac{\partial \rho'}{\partial t} = -\nabla\boldsymbol{\cdot}(\rho \boldsymbol{u}' + \rho' \boldsymbol{U}) + O(\rho' \boldsymbol{u}'), \tag{A3}$$

where $\boldsymbol{U}$ is the mean fluid velocity. The correlation function of density-density fluctuations $\langle \rho'(\boldsymbol{x})\, \rho'(\boldsymbol{y})\rangle$ is determined by the following equation:

$$\frac{\partial}{\partial t} \langle \rho'(\boldsymbol{x})\, \rho'(\boldsymbol{y})\rangle = -\rho \left[\nabla_i^{(y)} \langle \rho'(\boldsymbol{x})\, u_i'(\boldsymbol{y})\rangle + \nabla_i^{(x)} \langle \rho'(\boldsymbol{y})\, u_i'(\boldsymbol{x})\rangle\right] - \frac{\nabla_i\, \rho}{\rho} [\langle \rho'(\boldsymbol{x})\, u_i'(\boldsymbol{y})\rangle + \langle \rho'(\boldsymbol{y})\, u_i'(\boldsymbol{x})\rangle], \tag{A4}$$

which follows from Eq. (A3). Since $\langle \rho'(\boldsymbol{x})\, u_i'(\boldsymbol{y})\rangle$ is very small (it is of the order of O(Ma^2), where Ma is the Mach number, see Ref. [50]) and is nearly independent of the turbulent heat flux, the correlation functions of the density-density fluctuations or density-temperature fluctuations are much smaller than the correlation functions of the temperature-temperature fluctuations, i.e.,

$$\frac{1}{T^2}\, |\langle [\nabla^2 \theta(\boldsymbol{x})]\, \nabla^2 \theta(\boldsymbol{y})\rangle| \gg \frac{1}{\rho^2}\, |\langle [\nabla^2 \rho'(\boldsymbol{x})]\, \nabla^2 \rho'(\boldsymbol{y})\rangle|, \tag{A5}$$

$$\frac{1}{T}\, |\langle [\nabla^2 \theta(\boldsymbol{x})]\, \nabla^2 \theta(\boldsymbol{y})\rangle| \gg \frac{1}{\rho}\, |\langle [\nabla^2 \rho'(\boldsymbol{x})]\, \nabla^2 \theta(\boldsymbol{y})\rangle|, \tag{A6}$$

$$\frac{1}{T}\, |\langle [\nabla^2 \theta(\boldsymbol{x})]\, \nabla^2 \theta(\boldsymbol{y})\rangle| \gg \frac{1}{\rho}\, |\langle [\nabla^2 \theta(\boldsymbol{x})]\, \nabla^2 \rho'(\boldsymbol{y})\rangle|. \tag{A7}$$

In $\boldsymbol{k}$ space the correlation function $\langle \tau [\nabla^2 \theta(\boldsymbol{x})]\, [\nabla^2 \theta(\boldsymbol{y})]\rangle$ reads:

$$\langle \tau [\nabla^2 \theta(\boldsymbol{x})]\, [\nabla^2 \theta(\boldsymbol{y})]\rangle = \int \tau(k)\, k^4\, \langle \theta(\boldsymbol{k})\, \theta(-\boldsymbol{k})\rangle\, \exp(i\boldsymbol{k}\boldsymbol{\cdot}\boldsymbol{R})\, d\boldsymbol{k}. \tag{A8}$$

[1] A. Khain, M. Pinsky, T. Elperin, N. Kleeorin, I. Rogachevskii, and A. Kostinski, Atmosph. Res. **86**, 1 (2007).

[2] B. J. Devenish, P. Bartello, J.-L. Brenguier, L. R. Collins *et al.*, Quart. J. Roy. Meteorol. Soc. **138**, 1401 (2012).

[3] W. W. Grabowski and L.-P. Wang, Annu. Rev. Fluid Mech. **45**, 293 (2013).

[4] H. R. Pruppacher and J. D. Klett, *Microphysics of Clouds and Precipitation*, 2nd ed. (Kluwer Academic, Dordrecht, 1997).

[5] A. M. Blyth, S. G. Lasher-Trapp, W. A. Cooper, C. A. Knight, and J. Latham, J. Atmos. Sci. **60**, 2557 (2003).

[6] P. A. Vaillancourt, M. K. Yau, and W. W. Grabowski, J. Atmos. Sci. **58**, 1945 (2001).

[7] P. A. Vaillancourt, M. K. Yau, P. Bartello, and W. W. Grabowski, J. Atmos. Sci. **59**, 3421 (2002).

[8] P. Tisler, E. Zapadinsky, and M. Kulmala, Geophys. Res. Lett. **32**, L06806 (2005).

[9] L.-P. Wang, A. Orlando, B. Rosa, and W. W. Grabowski, New J. Phys. **10**, 075013 (2008).
[10] L.-P. Wang and M. R. Maxey, J. Fluid Mech. **256**, 27 (1993).
[11] T. Elperin, N. Kleeorin, and I. Rogachevskii, Phys. Rev. Lett. **77**, 5373 (1996).
[12] T. Elperin, N. Kleeorin, V. S. L'vov, I. Rogachevskii, and D. Sokoloff, Phys. Rev. E **66**, 036302 (2002).
[13] T. Elperin, N. Kleeorin, M. A. Liberman, V. S. L'vov, and I. Rogachevskii, Environ. Fluid Mech. **7**, 173 (2007).
[14] M. B. Pinsky and A. P. Khain, J. Aerosol Sci. **28**, 1177 (1997).
[15] M. B. Pinsky and A. P. Khain, Quart. J. Roy. Meteorol. Soc. **123**, 165 (1997).
[16] M. B. Pinsky and A. P. Khain, Quart. J. Roy. Meteorol. Soc. **128**, 501 (2002).
[17] M. B. Pinsky and A. P. Khain, J. Atmos. Sci. **61**, 1926 (2004).
[18] L.-P. Wang, A. S. Wexler, and Y. Zhou, J. Fluid Mech. **415**, 117 (2000).
[19] L.-P. Wang, O. Ayala, S. E. Kasprzak, and W. W. Grabowski, J. Atmos. Sci. **62**, 2433 (2005).
[20] Y. Zhou, A. S. Wexler, and L.-P. Wang, J. Fluid Mech. **433**, 77 (2001).
[21] J. Davila and J. C. R. Hunt, J. Fluid Mech. **440**, 117 (2001).
[22] Z. Dodin and T. Elperin, Phys. Fluids **14**, 2921 (2002).
[23] G. Falkovich, A. Fouxon, and M. G. Stepanov, Nature **419**, 151 (2002).
[24] S. Ghosh, J. Dávila, J. C. R. Hunt, A. Srdic, H. J. S. Fernando, and P. R. Jonas, Proc. Roy. Soc. London A **461**, 3059 (2005).
[25] K. Gustavsson and B. Mehlig, arXiv:1412.4374.
[26] K. D. Squires and J. K. Eaton, Phys. Fluids A **3**, 1169 (1991).
[27] M. Gavaises, A. Theodorakakos, G. Bergeles, and G. Breen, Proc. Inst. Mech. Eng. **210**, 465 (1996).
[28] P. Villedieu and O. Simonin, Comm. Math. Sci., Suppl. **1**, 13 (2004).
[29] C. Tang, P. Zhang, and C. K. Law, Phys. Fluids **24**, 022101 (2012).
[30] T. Elperin, N. Kleeorin, M. A. Liberman, and I. Rogachevskii, Phys. Fluids **25**, 085104 (2013).
[31] M. R. Maxey, J. Fluid Mech. **174**, 441 (1987).
[32] A. Eidelman, T. Elperin, N. Kleeorin, B. Melnik, and I. Rogachevskii, Phys. Rev. E **81**, 056313 (2010).
[33] J. Eggers, Rev. Mod. Phys. **69**, 865 (1997).
[34] J. Eggers, J. R. Lister, and H. A. Stone, J. Fluid Mech. **401**, 293 (1999).
[35] L. Duchemin, J. Eggers, and C. Josserand, J. Fluid Mech. **487**, 167 (2003).
[36] A. B. Nadykto, E. R. Shchukin, M. Kulmala, K. E. J. Lehtinen, and A. Laaksonen, Aerosol Sci. Technol. **37**, 315 (2003).
[37] H. Tennekes and J. L. Lumley, *A First Course in Turbulence* (The MIT Press, Cambridge, MA, 1973).
[38] T. Elperin, N. Kleeorin, and I. Rogachevskii, Phys. Rev. Lett. **76**, 224 (1996).
[39] B. Baker, J. Atmosph. Sci. **49**, 387 (1992).
[40] M. Pinsky and A. Khain, J. Appl. Meteorol. **40**, 1516 (2001); **42**, 65 (2003).
[41] A. B. Kostinski and R. A. Shaw, J. Fluid Mech. **434**, 389 (2001).
[42] R. A. Shaw, A. B. Kostinski, and M. L. Larsen, Q. J. R. Meteorol. Soc. **128**, 1043 (2002).
[43] K. Lehmann, H. Siebert, M. Wendisch, and R. A. Shaw, Tellus **59B**, 57 (2007).
[44] D. Etling and R. A. Brown, Boundary-Layer Meteorol. **65**, 215 (1993).
[45] B. W. Atkinson and J. Wu Zhang, Rev. Geophys. **34**, 403 (1996).
[46] A. G. Williams and J. M. Hacker, Boundary-Layer Meteorol. **61**, 213 (1992).
[47] M. Bukai, A. Eidelman, T. Elperin, N. Kleeorin, I. Rogachevskii, and I. Sapir-Katiraie, Phys. Rev. E **79**, 066302 (2009).
[48] J. H. Seinfeld and S. N. Pandis, *Atmospheric Chemistry and Physics. From Air Pollution to Climate Change*, 2nd ed. (John Wiley & Sons, New York, 2006).
[49] A. A. Lushnikov and M. Kulmala, Phys. Rev. E **70**, 046413 (2004).
[50] P. Chassaing, R. A. Antonia, F. Anselmet, L. Joly, and S. Sarkar, *Variable Density Fluid Turbulence* (Kluwer Academic, Dordrecht, The Netherlands, 2002).